PROCEEDINGS OF SPIE

SPIEDigitalLibrary.org/conference-proceedings-of-spie

# Adaptive inertia weight particle swarm algorithm for optimized hyperspectral image enhancement

Trongtirakul, Thaweesak, Agaian, Sos

Thaweesak Trongtirakul, Sos Agaian, "Adaptive inertia weight particle swarm algorithm for optimized hyperspectral image enhancement," Proc. SPIE 11734, Multimodal Image Exploitation and Learning 2021, 1173403 (12 April 2021); doi: 10.1117/12.2585548

SPIE.

Event: SPIE Defense + Commercial Sensing, 2021, Online Only

# Adaptive Inertia Weight Particle Swarm Algorithm for Optimized Hyperspectral Image Enhancement

Thaweesak Trongtirakul *[a], Sos Agaian[b]
[a]Faculty of Industrial Education, Rajamangala University of Technology Phra Nakhon, 399 Samsen Rd, Wachira Phayaban, Dusit, Bangkok, THAILAND 10300
[b]Dept. of Computer Science, College of Staten Island, 2800 Victory Blvd., Staten Island, NY USA 10314

## ABSTRACT

Hyperspectral images deliver several hundred spectral bands covering the visible and the infrared wavelength. Visualize hyperspectral information on a trichromatic display is impracticable to show information, which contains a hundred bands. Therefore, the selection of representative bands and the improvement of image quality are challenging tasks. In this paper, a simple, effective hyperspectral image visualization method based on hyperspectral image enhancement with the use of different cost functions is proposed. The proposed method consists of two major steps. First, the wavelength-based band selection chooses three subsets of adjacent hyperspectral bands. Second, the selected bands are improved by the proposed fractional contrast stretching algorithm with optimizations. In the nature-inspired optimization algorithm with an adaptive inertia weight, the quality of an enhanced image will be evaluated by different cost functions – image quality measures. This paper's main contribution is that: i) the selection of representative bands corresponding to natural-color appearance, ii) the image enhancement for visualization, and iii) the investigation of the suitable cost function for hyperspectral image visualization. Experiments performed on several hyperspectral datasets illustrate that the proposed method can produce remarkable visualization performance in subjective and objective assessments.

**Keywords:** Hyperspectral Image Enhancement, Hyperspectral Image Visualization, Wavelength-based Band Selection

## 1. INTRODUCTION

Hyperspectral imagery (HSI) delivers distinguished information that dominates the infrared and the visible wavelength spectrums [1-2]. With superior resolution, it contributes better the potentiality of diagnostics for feature classification, detection, and discrimination than conventional multi-spectral imagery. Nevertheless, it is challenging to visualize the numerous pieces of information contained in a hyperspectral cube [3]. The most widely used scheme is to employ three primary colors to represent an image scene's overview. However, hyperspectral imagery's high dimensionality delivers advanced challenges in image processing and data storage [4-5]. The visualization of hyperspectral scenes is beyond the possibility of illustrating information, which contains several hundreds of spectral bands using ordinary screens. Since the last decade, band selection methods have been proposed by handling the advantages of band redundancy to reduce the hyperspectral information's spectral bands while maintaining spatial information [6-8]. The primary objective of band selection approaches is to select three representative bands of several hundred hyperspectral scenes as primary colors, red, green, and blue components [9]. For example, Jia *et al.* propose a principal components transformation for hyperspectral remote sensing image display and classification [10]. This method's main idea is to divide hyperspectral imagery into several highly-related sub-groups and then reduce the data cube's spectral dimensionality using the principal component analysis (PCA) [10]. Su *et al.* introduce the spectral weighting envelopes based on a stretched version of the CIE1964 tristimulus Color Matching Functions (CMFs) [11]. The CIE 1964 tristimulus color matching envelopes were mapped to standard RGB (sRGB) color-space with its D65-white point [12]. However, these band above selection methods illustrate a low-contrast appearance. It requires a unique image processing tool to accomplish good visualization.

In this paper, we focus on using different cost functions for optimizing the quality of hyperspectral image visualization. The remainder of this paper is organized as follows. In Section 2, related to the proposed method, the adaptive inertia weight particle swarm algorithm for optimized hyperspectral image enhancement is introduced. In Section 3, computer simulation results are illustrated and compared with existing state-of-the-art visualization methods. After that, the effectiveness of the proposed method is discussed by image quality measures in Section 4. Finally, the conclusion is summarized in Section 5.

Multimodal Image Exploitation and Learning 2021, edited by Sos S. Agaian, Vijayan K. Asari, Stephen P. DelMarco, Sabah A. Jassim, Proc. of SPIE Vol. 11734, 1173403
 · doi: 10.1117/12.2585548

## 2. THE PROPOSED METHOD

Let $\mathbf{I} = \{I_{i,j,\lambda}\}$ denote a given hyperspectral cube composed of $l$ discrete grayscale levels denoted as $\{I_0, I_1, \ldots, I_{L-1}\}$, where $I_{i,j,\lambda}$ represents as the intensity of the image at the spatial location $(i,j)$ in the spectra band $(\lambda)$ and $I_{i,j,\lambda} \in \{I_0, I_1, \ldots, I_{L-1}\}$. This section describes the proposed adaptive inertia weight particle swarm algorithm for optimized hyperspectral image enhancement. The method contains two following major steps.

**Wavelength Based-Band Selection (WBS):** A hyperspectral cube contains several hundred distinctive and informative bands. Each band of the cube can illustrate one band as a grayscale image or a fusion of three bands as a color image. In digital image processing, the three primary colors (red, green, and blue) are in the wavelengths of 610–700 nm, 500–570 nm, 450–500 nm, respectively [11]. The WBS selection can present a true-color image by choosing several bands close to the wavelengths above. The wavelength based-band selection can be expressed by

$$\begin{bmatrix} R_{i,j} \\ G_{i,j} \\ B_{i,j} \end{bmatrix} = w_\lambda \cdot \begin{bmatrix} \{I_{i,j,\lambda} | \lambda = [610\text{nm}, 700\text{nm}]\} \\ \{I_{i,j,\lambda} | \lambda = [500\text{nm}, 570\text{nm}]\} \\ \{I_{i,j,\lambda} | \lambda = [450\text{nm}, 500\text{nm}]\} \end{bmatrix} \tag{1}$$

where $w_\lambda$ represents a function-based spectra weight ND where $R_{i,j}, G_{i,j}$ and $B_{i,j}$ denote a red component, a green component, and a blue component, respectively.

Occasionally, the composite color image illustrates a low-luminance appearance, but it also contains distinctive and informative data. For color visualization, the luminance level is considered and it can be computed by

$$X_{i,j,k} = \left( \begin{bmatrix} R_{i,j} \\ G_{i,j} \\ B_{i,j} \end{bmatrix} - \min\{R_{i,j}, G_{i,j}, B_{i,j}\} \right) \div \max\left\{ \begin{bmatrix} R_{i,j} \\ G_{i,j} \\ B_{i,j} \end{bmatrix} - \min\{R_{i,j}, G_{i,j}, B_{i,j}\} \right\} \tag{2}$$

**Fractional Nonlinear Contrast Stretching Mechanism:** Once a wavelength-based band selection hyperspectral image, $\boldsymbol{X_{i,j,k}}$, with extended color components, $\boldsymbol{k}$, of bands has been obtained from the band selection process. These $\boldsymbol{k}$ spectra bands follow a fractional contrast stretching process aiming to normalize local luminance levels on the Hue-Saturation-Value (HSV) color-space. First, the set of gamma parameters must be defined by the value (V) component's average brightness. The set of gamma parameter can be written as:

$$\gamma_n = \begin{cases} 0.1, 0.2, \ldots, 1.0, & \mu \leq 0.5 I_{L-1} \\ 1.1, 1.2, \ldots, 2.0, & \mu > 0.5 I_{L-1} \end{cases} ; n = 1, 2, \ldots, n \tag{3}$$

Depending on the global average brightness, $\mu$. Here, $I_{L-1}$ denotes the total number of brightness levels assigned to split the brightness based-class of an image. The use of different parameters, $\gamma_n$, in each class, attempts to generate uniform luminance passing through a nonlinear term. The general form of the fractional function is described by

$$V_{i,j,n} = \frac{\mu}{\sigma + \alpha} \left( (v_{i,j} - m_{i,j}) + m_{i,j} \right)^{\gamma_n} \tag{4}$$

where $v_{i,j}$ denotes the luminance component on an HSV color-space of the selected image, $X_{i,j,k}$. $m_{i,j}$ represents a local mean of $v_{i,j}$. $\sigma$ and $\alpha$ are the global standard deviation value and a small number to avoid the calculation error in case $\sigma$ equal to zero. $\gamma_n$ is a gamma correction parameter and $n$ is the index of $\gamma$.

The resulting of stretched images using the set of gamma parameters results in presenting several stretched images based on the number of parameters. It is necessary to fuse all stretched images with a reasonable proportion. The weighted fusion of stretched images can be expressed as:

$$\mathcal{V}_{i,j} = \omega_n \cdot V_{i,j,n} \;\; ; \;\; \sum_{a=1}^{n} \omega_a = 1.0 \tag{5}$$

where $V_{i,j,n}$ represents the set of the stretched value image component and $\omega_n$ denotes the set of optimal weights. It can be optimized by using the nature-inspired search algorithm such as the Particle Swarm Optimization (PSO) algorithm.

**Algorithm I:** Modified Particle Swarm Optimization (MPSO)

**Input:** luminance component, $v_{i,j}$

**Initialization:** Number of unknown variables $(n)$, Image cost function $f(v_{i,j})$, Personal acceleration coefficient $(c_1)$, Social acceleration coefficient $(c_2)$, number of iterations $(t)$, Population size $(P)$, the position of a weight $(\omega)$

**Optimization:** A group with $p$ particles is randomly initialized, assuming that the population is $a = (a_1, a_2, \dots, a_n)$ in a $d$-dimension search space.

**While**
- When particles move to a certain speed in the space, the position state property of particle $a$ is set as: $a_x = (a_{x1}, a_{x2}, \dots, a_{xd})$.
- The fitness values corresponding to each particle position can be calculated based on the cost function.
- The velocity vector, $s_x = (s_{x1}, s_{x2}, \dots, s_{xd})$, of particle $x$ is calculated as:
$$s_{xd}^{t+1} = w \cdot s_{xd}^{t} + c_1 \text{rand}[0,1](P_{xd}^{t} - a_{xd}^{t}) + c_2 \text{rand}[0,1]\left(P_{gd}^{t} - a_{xd}^{t}\right) \;\; ; \;\; w = t^{-1}$$
where $P_x = (P_{x1}, P_{x2}, \dots, P_{xd})$ represent a personal optimal position vector and $P_g = \left(P_{g1}, P_{g2}, \dots, P_{gd}\right)$ denotes a social position vector.
- The new position of particle $x$ is updated as:
$$a_{xd}^{k+1} = a_{xd}^{k} + s_{xd}^{t+1}$$
- Apply the social position vector as the set of optimal weights to the fractional nonlinear contrast stretching mechanism.
- Apply a local image enhancement algorithm, a color correction algorithm, and a denoising algorithm to the stretched image, respectively.
- Evaluate a resulting image using cost functions. (see Eq. 6-8)

**Until**
- The fitness value is satisfied.

**Output:** Enhanced Image

**Adaptive Inertial Weight in the Particle Swarm Optimization (PSO) Algorithm:** The outstanding PSO features are easy-to-implement, robust-to-control parameters, and inexpensive computation compared with other existing heuristic search algorithms. The inertia weight of PSO plays a vital role in balancing between an exploration process and an exploitation process. The inertia weight determines the participation rate of the previous speed and the current speed of particles. Therefore, the improvement of the inertia weight increases more efficiency in searching required parameters. In this paper, the adaptive inertia weight is applied to the modified PSO (MPSO) Algorithm 1.

**Cost Functions [14-15, 22-34]:** Cost functions play a vital role in constructing and designing image enhancement tools. In this paper, we used three image Cost functions. We will use Panetta *et al.* [14] the colorfulness (CF) Cost function, which is formulated as the variance ratio to the average chrominance in each color component.

$$f(I_{i,j,k}) = 0.02 \log\left(\frac{\sigma_\alpha^2}{|\mu_\alpha|^{0.2}}\right) \log\left(\frac{\sigma_\beta^2}{|\mu_\beta|^{0.2}}\right) \tag{6}$$

where $\alpha = R_{i,j} - G_{i,j}, \beta = 0.5\left(R_{i,j} + G_{i,j}\right) - B_{i,j}$ represent opponent spaces, and $\sigma_\alpha^2, \sigma_\beta^2, \mu_\alpha, \mu_\beta$ denote the variance and mean values along with these two opponent color spaces. $R_{i,j}, G_{i,j}$ and $B_{i,j}$ are red, green, and blue components, respectively.

**Cube Root Mean Enhancement (CRME) Measure:** It was introduced by Karen *et al.* in 2013 [14]. The concept of the CRME calculates the relative difference of the color cube center and the combination neighbor information in the local color cube.

$$f(I_{i,j}) = \frac{1000}{k_1 k_2} \sqrt{\sum_{i=1}^{k_1} \sum_{j=1}^{k_2} \left( \frac{\log \left| I_{i,j} - \sum_{c=1}^{3} \lambda_c \frac{I_{c1} + I_{c2} + \cdots + I_{cn}}{n} \right|}{\log \left| I_{i,j} + \sum_{c=1}^{3} \lambda_c \frac{I_{c1} + I_{c2} + \cdots + I_{cn}}{n} \right|} \right)^{\alpha}} \quad (7)$$

where $\lambda_c$ represents the weights for different color components, $\lambda_1 = 0.299, \lambda_2 = 0.587$, and $\lambda_3 = 0.114$. $\alpha$ is assigned (7) to the ratio based on the region to which the local background of the current cube belongs, the DeVries-Rose region, $\alpha = 0.2$, the Weber region, $\alpha = 0.4$, and the Saturation region, $\alpha = 0.8$. $I_{i,j}$ denote an image.

**Average Gradient (AG) [15]:** This measure is formulated as the directional change (edge information) in the intensity of color images.

$$f(I_{i,j}) = \frac{1}{M \times N} \sum_{i=1}^{N-1} \sum_{j=1}^{M-1} \sqrt{\frac{G(I_{i,j} - I_{i+1,j})^2 + G(I_{i,j} - I_{i,j+1})^2}{2}} \quad (8)$$

where $M$ and $N$ are the numbers of rows and columns of the image, $I_{i,j}$. $G(I_{i,j} - I_{i+1,j})$ and $G(I_{i,j} - I_{i,j+1})^2$ denote the gradient vector of the image in rows and columns, respectively.

## 3. COMPUTER SIMULATION RESULTS

This work selects four hyperspectral images to illustrate the effectiveness of the proposed method. The method is implemented by MATLAB® online. The hyperspectral data is captured by SPECIM hyperspectral camera and multiple consumer cameras. The datasets are available on the Hyperspectral & Color Imaging database [16]. The dataset provides a spatial resolution of 1312×1903 with 49 bands, covering a spectral range of 401.01nm-698.41nm. Figure 1 displays the color image captured by a commercial camera correspond to its hyperspectral data.

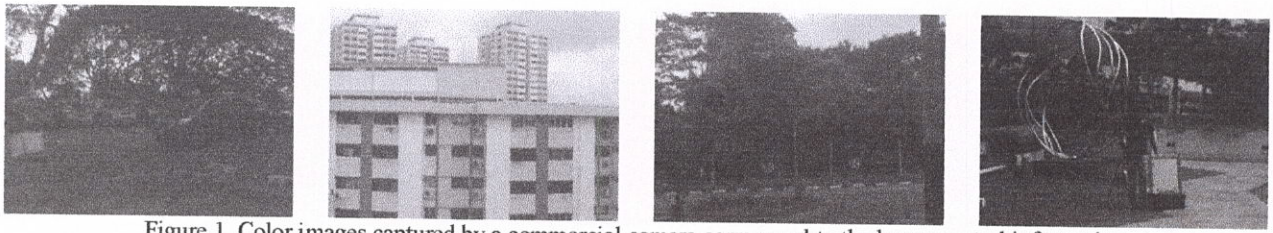

Figure 1. Color images captured by a commercial camera correspond to the hyperspectral information

**Visualization Results of Different Cost Functions:** in this sub-section, the proposed hyperspectral image visualization approach using different cost functions is compared with the several widely used visualization methods, including the PCA and CMF methods.

The visualization results of different methods are presented in Figure 2. Furthermore, an extracted view is presented under each image. As shown in this figure, the PCA method chooses three bands from the original hyperspectral cube, the surface of the resulting image illustrates a hazy phenomenon. For the CMF and the wavelength-based band selection methods, the color differences belonging to different ground information become more apparent, but spatial details cannot be created distinctly. The resulting images of the proposed method with varying cost functions produce satisfactory visualization results with distinct scene details. Among the three other cost functions, the CF method illustrates visibly outstanding information and preserves details well.

The second experiment is performed on scene no. 18 – 'building' as shown in Figure 3. In this illustrative example, the PCA method wields a similar result that it illustrates a hazy phenomenon. For the CMF method, the boundaries of different details are slight clear, but it is not colorful. For the wavelength-based band selection method, the resulting image possesses a better contrast than the PCA method and the CMF method. Also, the colors tend to be more natural. The resulting images of the proposed method with the CRMS cost function illustrate the details under dark regions well by visualization.

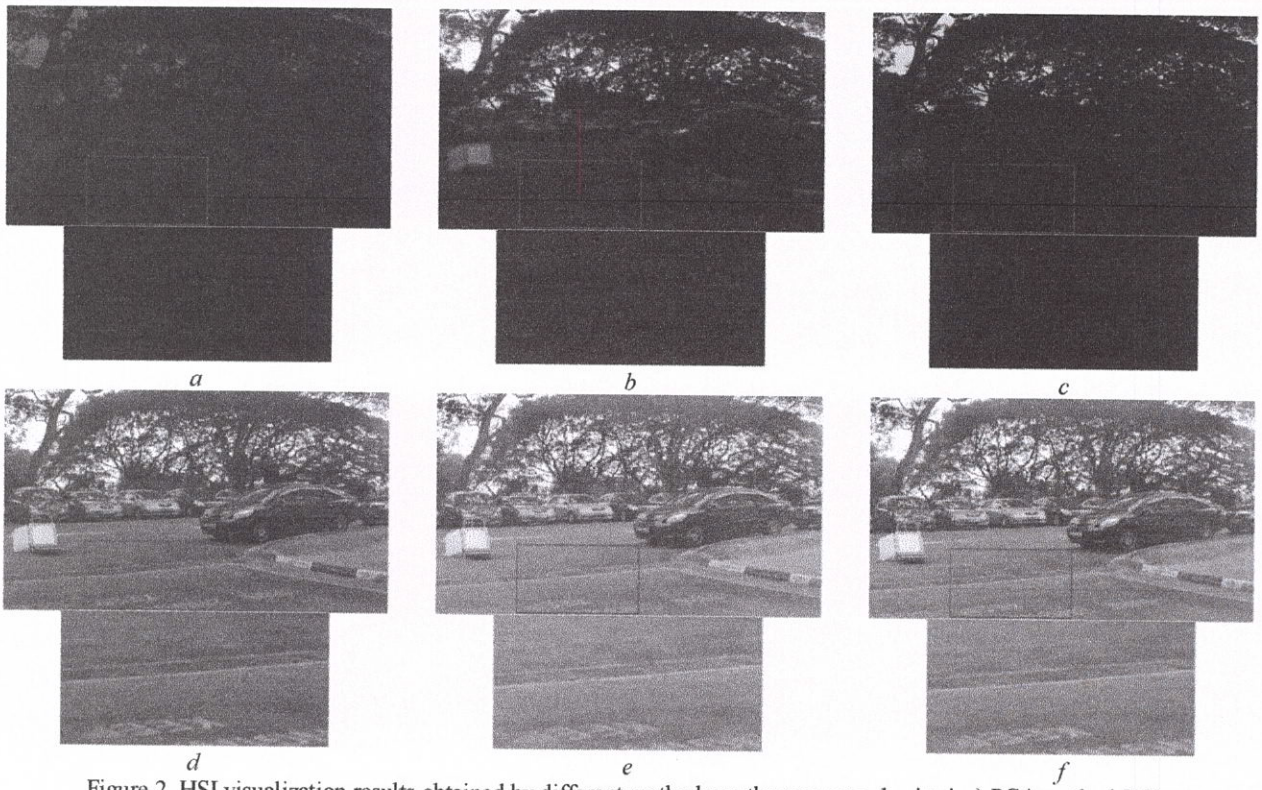

Figure 2. HSI visualization results obtained by different methods on the scene no. 1 – 'car': a) PCA method [10]; b) CMF method [11]; c) Wavelength-based band selected image; d) AG method; e) CF method; f) CRMS method.

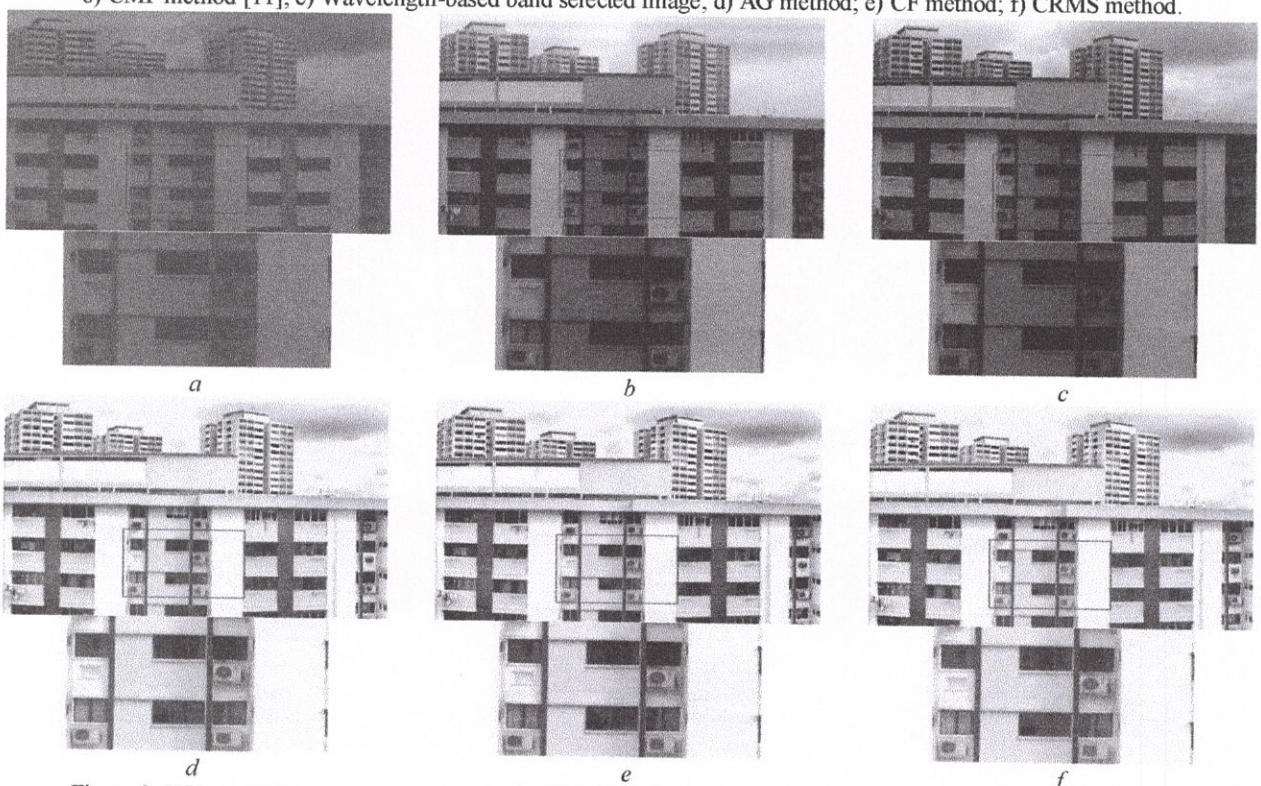

Figure 3. HSI visualization results obtained by different methods on scene no. 18 – 'building': a) PCA method [10]; b) CMF method [11]; c) Wavelength-based band selected image; d) AG method; e) CF method; f) CRMS method.

Figure 4. HSI visualization results obtained by different methods on scene no. 28 – 'man': a) PCA method [10]; b) CMF method [11]; c) Wavelength-based band selected image; d) AG method; e) CF method; f) CRMS method.

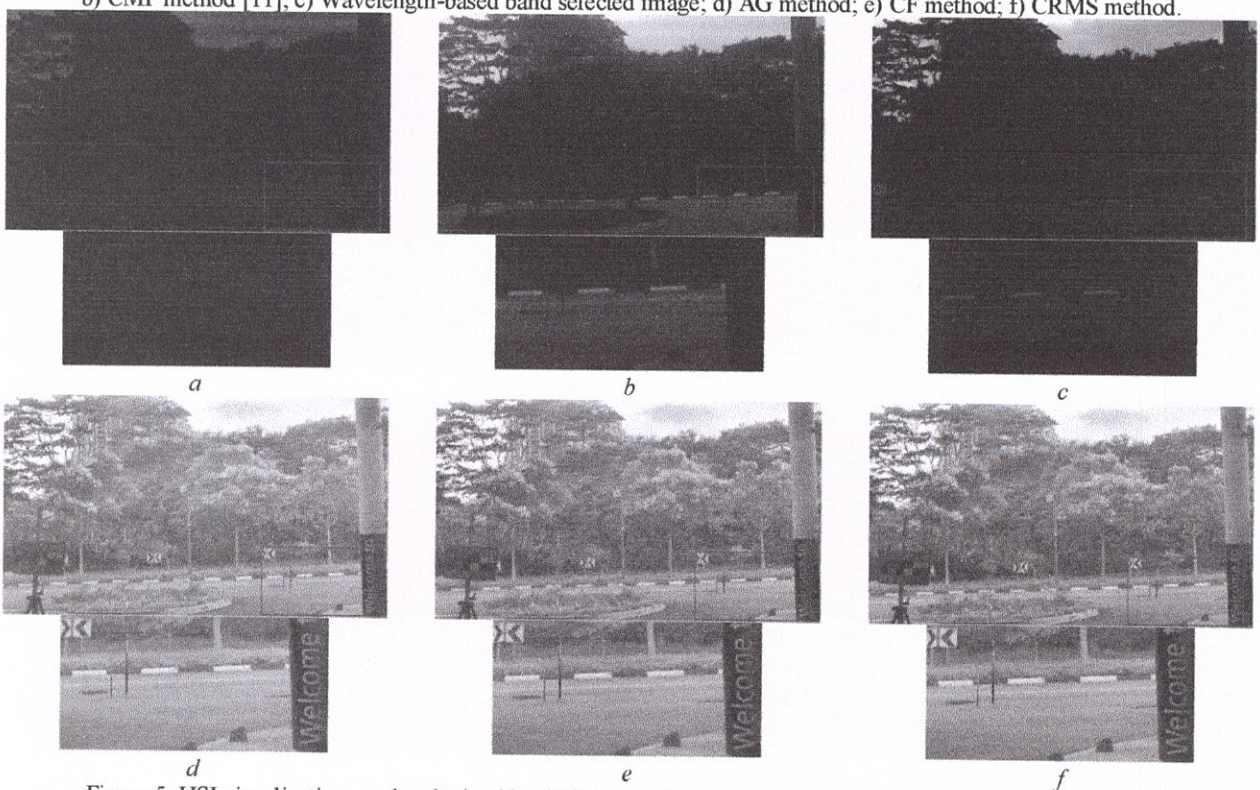


Figure 5. HSI visualization results obtained by different methods on scene no. 34 – 'street': a) PCA method [10]; b) CMF method [11]; c) Wavelength-based band selected image; d) AG method; e) CF method; f) CRMS method.

The third experiment is performed on scene no. 28 – 'man.' The resulting image obtained by different methods is illustrated in Figure 4. The PCA method appears as a hazy severe phenomenon. For the CMF method and the wavelength-based band selection method, the resulting images have a slight improvement in preserving spatial details. Still, the CMF method is likely to be colorless. However, the proposed method's results optimized by three different cost functions is better than those of the other compared methods. The proposed method still produces satisfactory results in preserving the color detail discriminability, such as the color chart, trees, garden paths, and walkways.

The last experiment is performed on scene no. 34 – 'street.' The resulting image obtained by different methods is presented in Figure 5. The PCA method fails to present specific information. For the CMF method, the result preserves outstanding information, but most colors are washed out. The CMF method improves the clarity of the whole image, but it still suffers from the loss of colorfulness. For the wavelength-based band selection method, the spatial details are not able to be represented evidently. The luminance of the resulting image appears as a lowlight phenomenon. The resulting images obtained by the proposed method outperform those of the other compared methods. Following the previous experimental results performed on scene no. 1, no. 18, and no. 28. Moreover, the proposed method optimized by the CRMS cost function produces a satisfactory result in highlighting the unseen details while preserving natural colors.

## 4. EFFECTIVENESS

To evaluate the visualization performance of different methods, commonly used quality metrics, i.e., entropy information (EI), a combination of enhancement by entropy (CEME), and a combination of contrast, energy, and entropy (CEE), are adopted. For each of the metrics, a larger value indicates a better visualization performance.

***Entropy Information (EI):*** it refers to the degree of information in an image [17-20].

$$f(I_{i,j}) = -\sum_{x=1}^{L-1} p_x \log_2(p_x) \tag{9}$$

where $p_x$ is the probability density function of an image, $I_{i,j}$, and $L$ represents the number of discrete grayscale levels.

***Combination of enhancement by entropy (CEME):*** this measure was aimed to introduce to resolve some limitation of enhancement measure by entropy (EME). The EME works well for low-contrast and lowlight conditions, while the CEME takes the same conceptual formulation and focuses on normalized luminance conditions [21]. The measure is formulated as the local minimum ratio to the local maximum metrics in each color component.

$$f(I_{i,j}) = \frac{1}{k_1 k_2} \sum_{i=1}^{k_1} \sum_{j=1}^{k_2} \max\{EEME(I_{i,j}), MEEME(I_{i,j})\} \tag{10}$$

$$EEME(I_{i,j}) = -\frac{20}{3.1808}\left(\frac{[I_{max}]_{i,j}^{m,n} - [I_{min}]_{i,j}^{m,n}}{[I_{max}]_{i,j}^{m,n} + [I_{min}]_{i,j}^{m,n}}\right) \log\left(\frac{[I_{max}]_{i,j}^{m,n} - [I_{min}]_{i,j}^{m,n}}{[I_{max}]_{i,j}^{m,n} + [I_{min}]_{i,j}^{m,n}}\right) \tag{11}$$

$$MEEME(I_{i,j}) = -\frac{1}{54.1344}\left([I_{max}]_{i,j}^{m,n} - [I_{min}]_{i,j}^{m,n}\right) \log\left(\frac{[I_{max}]_{i,j}^{m,n} - [I_{min}]_{i,j}^{m,n}}{[I_{max}]_{i,j}^{m,n} + [I_{min}]_{i,j}^{m,n}}\right) \tag{12}$$

where $[I_{min}]_{i,j}^{m,n}$ and $[I_{max}]_{i,j}^{m,n}$ represent the local minimum and maximum intensity metric. $m \times n$ denotes the block size of a local tile. $k_1, k_2$ are the size of an image, $I_{i,j}$.

***Combination of Contrast, Energy, and Entropy (CCE):*** this measure combines two image attributes, contrast, and energy, through gray level co-occurrence metrics with entropy information [18,22].

$$f(I_{i,j}) = \log\left(\frac{e^{I_C} e^{H(I_{i,j})}}{I_E}\right) \tag{13}$$

$H(I_{i,j})$ is an entropy value of an enhanced image, $I_{i,j}$. $I_C$ and $I_E$ denote the contrast and energy of gray level co-occurrence metrics.

The objective evaluations of the visualization results are illustrated in Table 1. It can be noted from Table 1 that the most results yielded by the proposed visualization method are more distinguished than those obtained by the compared methods in terms of EI, CEME, and CEE, which further stimulates the effectiveness of the proposed method. Also, the proposed method with three different cost functions produces different EI, CEME, and CEE values. Among the use of other cost functions, AG, CF, and CRMS measures, the CF cost function's proposed method yields the highest sum values of EI, CEME, and CEE. The proposed methods with the CRMS cost function and the AG cost function follow closely behind. The proposed method with the CF cost function can visualize spatial information and the spectral contrast more productively.

For scene no. 18, the luminance of the proposed images is likely to be brighter. The saturation of brightness might degrade some information. The informative quality partially vanishes. It is noticeable from the entropy information value

Table 1. Objective Evaluation of the PCA, the CMF, and the Proposed Methods

| Method | Scene No.1 'car' | | | Scene No.18 'building' | | | Scene No.28 'man' | | | Scene No.34 'street' | | |
|---|---|---|---|---|---|---|---|---|---|---|---|---|
| | EI | CEME | CEE | EI | CEME | CEE | EI | CEME | CEE | EI | CEME | CEE |
| Original | 5.08 | 3.24 | 2.33 | 7.66 | 21.33 | 4.16 | 6.63 | 11.51 | 3.34 | 5.40 | 4.58 | 2.48 |
| PCA [10] | 3.24 | 7.10 | 1.51 | 5.95 | 24.85 | 2.90 | 5.13 | 11.47 | 2.40 | 3.45 | 4.93 | 1.55 |
| CMF [11] | 6.35 | 7.80 | 3.26 | 7.77 | 18.81 | 4.27 | 6.95 | 9.11 | 3.68 | 6.63 | 6.95 | 3.34 |
| Proposed with AG | 6.99 | 16.72 | 3.79 | 6.93 | 27.43 | 3.71 | 7.64 | 30.32 | 4.38 | 7.16 | 23.45 | 3.94 |
| Proposed with CF | 7.07 | 21.73 | 3.91 | 7.10 | 27.33 | 3.84 | 7.65 | 30.50 | 4.38 | 7.21 | 21.71 | 3.94 |
| Proposed with CRMS | 7.11 | 19.22 | 3.91 | 6.91 | 27.93 | 3.69 | 7.64 | 30.10 | 4.38 | 7.25 | 21.44 | 3.98 |

## 5. CONCLUSION

The paper introduces a simple, effective hyperspectral image visualization method based on optimized image enhancement using adaptive inertia weight particle swarm algorithm, consisting of the following steps: the wavelength-based band selection method and a nonlinear contrast stretching function with different cost functions, AG, CF, and CRMS. The computer simulation results demonstrate outstanding performance in terms of entropy information (EI), color contrast indicated by the combination of enhancement measure by entropy (CEME), and the combination of contrast, energy, and contrast (CCE) through Gray Level Co-occurrence Metrics (GLCMs). The visualization results illustrate a superior natural appearance with high contrast information.

## REFERENCES


[1] G. Gigli, E. Bossé, and G.A. Lampropoulos, "An optimized architecture for classification combining data fusion and data-mining," *Inf. Fusion*, 8 (4) (2007) 366–378.

[2] L. Bruzzone, R. Cossu, and G. Vernazza, "Combining parametric and non-parametric algorithms for a partially unsupervised classification of multitemporal remote-sensing images," *Inf. Fusion*, 3 (4) (2002) pp. 289–297.

[3] Q. Du *et al.*, "Color display for hyperspectral imagery," *IEEE Trans. Geosci. Remote Sens.*, vol. 46, no. 6, pp. 1858–1866, 2008.

[4] W. Liu *et al.*, "Multiview dimension reduction via Hessian multiset canonical correlations," *Inf. Fusion*, vol. 41, pp. 119–128, 2018.

[5] R.S. Lynch, and P.K. Willett, "Use of Bayesian data reduction for the fusion of legacy classifiers," *Inf. Fusion*, vol. 4 no.1, pp 23–34, 2003.

[6] K. Kotwal, and S. Chaudhuri, "A Bayesian approach to visualization-oriented hyperspectral image fusion," *Inf. Fusion*, vol.14, no. 4, pp. 349-360, 2013.

[7] Q. Du, J.M. Bioucas-Dias, and A. Plaza, "Hyperspectral band selection using a sparse collaborative model," *IEEE International Conference Geoscience Remote Sensing. Symposium*, pp. 3054–3057, 2012.

[8] Y. Gu *et al.*, "Nonlinear multiple kernel learning with multiple-structure-element extended morphological profiles for hyperspectral image classification," *IEEE Trans. Geoscience Remote Sensing*, vol. 54, pp. 3235-3247, 2016.

[9] H. Su, Q. Du, and P. Du, "Hyperspectral image visualization using band selection," *IEEE Journal of Selected Topics in Applied Earth Observations and Remote Sensing*, vol. 7, no. 6, pp. 2647-2658, 2014.

[10] X. Jia, and J.A. Richards, "Segmented principal components transformation for efficient hyperspectral remote sensing image display and classification," *IEEE Trans. in Geoscience and Remote Sensing*, vol. 37, vol. 1, pp. 538–542, 1999.
[11] H. Su, Q. Du, and P. Du, "Hyperspectral Image Visualization Using Band Selection," in *IEEE Journal of Selected Topics in Applied Earth Observations and Remote Sensing*, vol. 7, no. 6, pp. 2647-2658, June 2014.
[12] Q. Du, and C.-I Chang, "Linear constrained distance-based discriminant analysis for hyperspectral image classification," *Pattern Recognition*, vol. 34, no. 2, pp. 361–373, 2001.
[13] J. C. Bansal et al., "Inertia Weight strategies in Particle Swarm Optimization," *Third World Congress on Nature and Biologically Inspired Computing*, Salamanca, pp. 633-640, 19 October 2011.
[14] K. Panetta, C. Gao, and S. Agaian, "No reference color image contrast and quality measures," in *IEEE Transactions on Consumer Electronics*, vol. 59, no. 3, pp. 643-651, August 2013.
[15] Y. Yuan, G. Zhu, and Q. Wang, "Hyperspectral Band Selection by Multitask Sparsity Pursuit," in *IEEE Transactions on Geoscience and Remote Sensing*, vol. 53, no. 2, pp. 631-644, Feb. 2015.
[16] Hyperspectral & Color Imaging, https://sites.google.com/site/hyperspectralcolorimaging/dataset/general-scenes
[17] P. Shanmugavadivu et al., "Particle swarm optimized bi-histogram equalization for contrast enhancement and brightness preservation of images," *The Visual Computer*, vol. 30, pp. 387-399, 2014.
[18] K. Dhal, and S. Das, "Cuckoo search with search strategies and proper objective function for brightness preserving image enhancement," *Pattern Recognition and Image Analysis*, vol. 27, pp. 695-712, 2017.
[19] W. Minjie *et al.*, "Particle swarm optimization-based local entropy weighted histogram equalization for infrared image enhancement," *Infrared Physics & Technology*, vol. 91, pp. 164-181, 2018.
[20] P. Babu, and V. Rajamani, "Contrast enhancement using real coded genetic algorithm based modified histogram equalization for grayscale images," *Inter. Journal of Imaging Systems & Technology*, no.1, pp.24-32, 2015.
[21] T. Trongtirakul *et al.*, "Nonlinear contrast stretching with optimizations," *Proc. SPIE, Mobile Multimedia/Image Processing, Security, and Applications 2019*, 1099303, 13 May 2019.
[22] K. Dhal, and S. Das, "Local search based dynamically adapted Bat Algorithm in image enhancement domain," *International Journal of Computing Science and Mathematics*, vol. 11, no. 1, pp. 1-28, 27 February 2020.
[23] S. Agaian, "Visual morphology," *Proc. SPIE 3646, Nonlinear Image Processing X*, 5 March 1999.
[24] B. Silver, S. Agaian and K. Panetta, "Contrast entropy based image enhancement and logarithmic transform coefficient histogram shifting," *Proceedings. (ICASSP '05)*, vol. 2, pp. ii/633-ii/636, 2005.
[25] R. Kogan at al., visualization using rational morphology and zonal magnitude reduction", *Proc. SPIE 3304, Nonlinear Image Processing IX*, 6 April 1998.
[26] L. Lu *et al.*, "Comparative study of histogram equalization algorithms for image enhancement," *Proc. SPIE 7708, Mobile Multimedia/Image Processing, Security, and Applications*, 2010.
[27] A. Grigoryan, and S. Agaian, "Quaternion and octonion color image processing with MATLAB," SPIE 2018.
[28] A. Grigoryan, and S. Agaian, "Retooling of Color Imaging in the Quaternion Algebra," *Applied Mathematics and Sciences: An International Journal (MathSJ)*, vol. 1, no. 3, December 2014.
[29] J. K. Ratzloff *et al.*, "Robotilter: an automated lens/CCD alignment system for the Evryscope," *Journal of Astronomical Telescopes, Instruments, and Systems* 6(1), 018002 (29 January 2020).
[30] D. A. Rowlands, "Equivalence theory for cross-format photographic image quality comparisons," *Optical Engineering* 57(11), 110801 (16 November 2018).
[31] X. Liu *et al.*, "Performance evaluation of no-reference image quality metrics for face biometric images," *Journal of Electronic Imaging* 27(2), 023001 (2 March 2018).
[32] R. S. Allison *et al.*, "Perspectives on the definition of visually lossless quality for mobile and large format displays," *Journal of Electronic Imaging* 27(5), 053035 (11 October 2018).
[33] C. Snyder *et al.*, "Algorithm development for intrafraction radiotherapy beam edge verification from Cherenkov imaging," *Journal of Medical Imaging* 5(1), 015001 (2 January 2018).
[34] S. C. Pei *et al.*, "Single image desmoking using haze image model and human visual system," *Journal of Electronic Imaging* 28(4), 043007 (11 July 2019).